Regular black holes: Guilfoyle's electrically charged solutions with a perfect fluid phantom core

José P. S. Lemos
Centro Multidisciplinar de Astrofísica (CENTRA),
Departamento de Física,
Instituto Superior Técnico (IST),
Universidade de Lisboa (UL),
Avenida Rovisco Pais 1, 1049-001 Lisboa, Portugal
Email: joselemos@ist.utl.pt

Vilson T. Zanchin
Centro de Ciências Naturais e Humanas,
Universidade Federal do ABC,
Avenida dos Estados 5001, Santo André,
09210-580 São Paulo, Brazil
Email: zanchin@ufabc.edu.br

arXiv:1603.07359v2 [gr-qc] 28 Jun 2016

Regular black hole solutions are found among the Guilfoyle exact solutions. These are spherically symmetric solutions of general relativity coupled to Maxwell's electromagnetism and charged matter where the metric potentials and electromagnetic fields are related in some particularly simple form. We show that, for certain ranges of the parameters, there are objects which correspond to regular charged black holes, whose interior region is filled by an electrically charged phantomlike fluid, or, in the limiting case, a de Sitter false vacuum fluid, and whose exterior region is Reissner-Nordström. The boundary between both regions is a smooth boundary surface, except in the limiting case where the boundary is made of a massless electrically charged spherically symmetric coat. The main physical and geometrical properties of such charged regular solutions are analyzed.

PACS numbers: 04.70.Bw, 04.20.Jb, 04.40.Nr, 04.40.Dg

Keywords: Regular black holes; null and timelike boundaries; Einstein-Maxwell equations

I. INTRODUCTION

Solutions of Einstein-Maxwell with matter equations are of importance as they not only represent a class of solutions in general relativity but also give hints to the behavior of solutions with other type of fields. Electric charged compact objects, starlike, solutions have been constructed by Guilfoyle in [1]. The interpretation of the fluid content in these solutions has appeared in [2], and part of the spectrum of the solutions received a global interpretation in [3, 4].

On the other hand, a class of compact objects that has been of interest are regular black holes, i.e., black holes that, contrary to the usual Schwarzschild and Reissner-Nordström black holes, do not possess curvature singularities at the center. In these regular black holes a well-behaved interior replaces the singularity.

The first work on regular black holes is due to Bardeen [5] whose regular black hole was put on a firm footing in [6]. Dymnikova [7] constructed a regular black hole solution whose interior matter is an anisotropic fluid obeying a de Sitter equation of state, $p = -\rho$, where ρ and p are the energy density and pressure of the fluid, respectively, that asymptotically approached the Schwarzschild spacetime. Other regular black hole solutions have been found in [8, 9] where the interior region is a de Sitter core that can be matched to a Reissner-Nordström exterior metric thanks to an energyless charged layer at the boundary surface (see also [10]). Regular black holes with nonlinear electrodynamics sources appear in, e.g., [11–13]. Stability of these black holes appeared in [14, 15]. Regular black holes in different theories of gravity also appeared in [16, 17], and in nonminimal theories in [18].

An important class of regular black holes is the class of phantom matter black holes. Phantom matter is characterized by a perfect fluid for which $\rho + p < 0$. Fluids satisfying such a condition may represent the dark energy sector of the Universe. The property of phantom matter to act as a negative effective mass turns it into a natural candidate to build models of compact objects and, in particular, to build black hole solutions free from singularities. This motivated several works reporting on black holes with phantom matter, some of them regular, see [19–28].

Now, electric charged matter provides repulsion, but in general this electric repulsion is not enough to furnish regularity at the center. However, electrically charged matter made of a phantom perfect fluid might indeed be suitable to produce enough antigravity in order to form a regular core. Thus it is worth exploring the possibility that the Guilfoyle solutions [1] contain a subset of regular

electrical black holes with a phantom perfect fluid core.

In the present work we analyze in detail the Guifoyle model for electrically charged matter [1] and show that within a certain range of the parameters of the model there are indeed regular black holes whose central core is made by a charged perfect fluid obeying an equation of state representing phantom matter for which $p+\rho<0$.

The layout of the paper is as follows. In Sec. II we present the basic equations describing a spherically symmetric electrically charged perfect fluid matter distribution satisfying some simplifying assumptions, that define the systems. We give explicitly the interior and exterior solutions with the appropriate boundary conditions and display the class of the Guilfoyle solutions that is of interest here. We also show the conditions on the solutions necessary to make them black holes. Section III is dedicated to analyzing the phantom regular charged black hole solutions we have found, presenting their main properties, and comparing the present solutions to other regular black hole solutions found in the literature. In Sec. IV a particular limit of the regular black holes analyzed, where the core is made of de Sitter material and there is a massless charged layer at the Cauchy horizon, is studied. Then in Sec. V the spectrum of the free parameters of the solutions that yields regular black holes is analyzed in detail. In the first part, we study the behavior of the mass and other free parameters in terms of the radius and energy density of the solutions. The second part contains the display of the regions of the parameter space where regular black holes can be found. We also comment on some interesting cases including the ones analyzed in the previous sections. Finally, in Sec. VI we conclude.

II. GUILFOYLE SOLUTIONS AND BLACK HOLE CONDITIONS

A. Spherical static Weyl-Guilfoyle systems and equations

The matter source is a static charged fluid distribution with spherical symmetry. The metric is conveniently written in the form

$$ds^2=-B(r)\,dt^2+A(r)\,dr^2+r^2\,(d\theta^2+\sin^2 d\varphi^2)\,, \quad (1)$$

where $(t,\,r,\,\theta,\,\varphi)$ are spherical symmetric coordinates, and the functions A and B depend on the radial coordinate r only. The fluid is characterized by its energy density $\rho_{\rm m}(r)$, isotropic pressure $p(r)$, electric charge density $\rho_{\rm e}(r)$, and four-velocity $U_\mu=-\sqrt{B(r)}\,\delta^t_\mu$. The electromagnetic gauge field $\mathcal{A}_\mu$ assumes the form

$$\mathcal{A}_\mu=-\phi(r)\,\delta^t_\mu\,, \quad (2)$$

where $\phi(r)$ is the electric potential.

Two important auxiliary quantities are the mass $M(r)$ inside a sphere of radius r

$$M(r)=\int_0^r 4\pi\,r^2\left(\rho_m(r)+\frac{Q^2(r)}{8\pi\,r^4}\right)dr+\frac{Q^2(r)}{2\,r}\,, \quad (3)$$

and the electric charge $Q(r)$ inside a sphere of radius r,

$$Q(r)=4\pi\int_0^r \rho_{\rm e}(r)\sqrt{A(r)}\,r^2 dr\,. \quad (4)$$

The system we study here is a case of the Weyl-Guilfoyle-type systems for which the metric potential $B(r)$ and the electric potential $\phi(r)$ are functionally related through a particular Weyl-Guilfoyle relation [1] (see also [2]), namely, $B(r)=a\,[-\epsilon\,\phi(r)+b]^2$, with a and b being arbitrary constants and $\epsilon=\pm1$. Now, the parameter b can be absorbed into the electric potential ϕ, and so without loss of generality one can set $b=0$. Thus,

$$B(r)=a\phi^2(r)\,, \quad (5)$$

with a being an arbitrary constant called the Guilfoyle parameter.

Using the Einstein-Maxwell equations one finds the set of equations for this system (we use units in which the gravitational constant and the speed of light are set to one). The Einstein part of the equations furnishes the following relations,

$$\frac{B'(r)}{B(r)}+\frac{A'(r)}{A(r)}=8\pi r\,A(r)\Big[\rho_{\rm m}(r)+p(r)\Big]\,, \quad (6)$$

$$\left(\frac{r}{A(r)}\right)'=1-8\pi\,r^2\left(\rho_{\rm m}(r)+\frac{Q^2(r)}{8\pi r^4}\right)\,, \quad (7)$$

where a prime denotes the derivative with respect to the radial coordinate r. With the definition of the total charge $Q(r)$ inside a sphere of radius r, see Eq. (4), the only nonzero component of the Maxwell equation yields $Q(r)=\frac{r^2\,\phi'(r)}{\sqrt{B(r)\,A(r)}}$, where an integration constant was set to zero. From Eq. (5) we can write $\phi(r)$ in terms of $B(r)$ as $\epsilon\phi(r)=\sqrt{\dfrac{B(r)}{a}}$. With this, the amount of electric charge inside a spherical surface of radius r, Eq. (4), is then given by

$$Q(r)=\frac{-\epsilon\,r^2\,B'(r)}{2\sqrt{aA(r)}\,B(r)}\,. \quad (8)$$

The electric charge is then obtained once we have the metric functions $B(r)$ and $A(r)$.

One of the equations, (6) or (7), can be interchanged with the contracted Bianchi identity equation, i.e., the conservation equation given here by

$$2p'(r)+\frac{B'(r)}{B(r)}\Big[\rho_{\rm m}(r)+p(r)\Big]-2\frac{\phi'(r)\rho_{\rm e}(r)}{\sqrt{B(r)}}=0\,. \quad (9)$$

B. Guilfoyle solutions

1. Interior solution

The interior goes up to a certain radius r_0, say. Guilfoyle's solutions are found under the assumption that the effective energy density $\rho_{\rm m}(r) + \dfrac{Q^2(r)}{8\pi\, r^4}$ is a constant,

$$8\pi\,\rho_{\rm m}(r) + \frac{Q^2(r)}{r^4} = \frac{3}{R^2}\,, \tag{10}$$

where R, a characteristic length associated to the inverse of the total energy density, is a constant to be related to the parameters of the exterior solution, m and q, by the junction conditions of the metric at the surface $r = r_0$. With this hypothesis, Guilfoyle [1] found an exact solution given by

$$A(r) = \left(1 - \frac{r^2}{R^2}\right)^{-1}\,, \tag{11}$$

$$B(r) = \left[\frac{(2-a)^2}{a^2}\,F^2(r)\right]^{a/(a-2)}\,, \tag{12}$$

$$\phi(r) = \epsilon\sqrt{\frac{B(r)}{a}} \tag{13}$$

$$8\pi\rho_{\rm m}(r) = \frac{3}{R^2} - \frac{a}{(2-a)^2}\frac{k_0^2}{R^4}\,\frac{r^2}{F^2(r)}\,, \tag{14}$$

$$\begin{aligned} 8\pi p(r) \;&=\; -\frac{1}{R^2} + \frac{a}{(2-a)^2}\frac{k_0^2}{R^4}\,\frac{r^2}{F^2(r)} + \\ &+\frac{2a}{2-a}\frac{k_0}{R^2}\,\frac{\sqrt{1-r^2/R^2}}{F(r)}\,, \end{aligned} \tag{15}$$

$$4\pi\rho_{\rm e}(r) = \frac{\epsilon\sqrt{a}}{2-a}\,\frac{k_0^2}{R^4}\,\frac{r^2}{F^2(r)}\left(1 + \frac{3F(r)\sqrt{1-r^2/R^2}}{k_0 r^2}\right). \tag{16}$$

The auxiliary functions are

$$M(r) = \frac{r^3}{2R^2} + \frac{a}{2\,(2-a)^2}\frac{k_0^2}{R^4}\,\frac{r^5}{F^2(r)}, \tag{17}$$

$$Q(r) = \frac{\epsilon\sqrt{a}}{2-a}\,\frac{k_0}{R^2}\,\frac{r^3}{F(r)}\,. \tag{18}$$

The function $F(r)$ is defined by

$$F(r) = k_0\sqrt{1 - \frac{r^2}{R^2}} - k_1\,, \tag{19}$$

and the integration constants k_0 and k_1 are given by

$$k_0 = \frac{R^2}{r_0^2}\left(\frac{m}{r_0} - \frac{q^2}{r_0^2}\right)\left(1 - \frac{r_0^2}{R^2}\right)^{-1/a}\,, \tag{20}$$

$$k_1 \;= k_0\sqrt{1 - \frac{r_0^2}{R^2}}\left[1 - \frac{a}{2-a}\frac{r_0^2}{R^2}\left(\frac{m}{r_0} - \frac{q^2}{r_0^2}\right)^{-1}\right], \tag{21}$$

where

$$m \equiv M(r_0)\,, \tag{22}$$

$$q \equiv Q(r_0)\,. \tag{23}$$

The constants k_0 and k_1 are found through the junction conditions. As one can check, the above solution is valid for all $a > 0$, the limiting case $a \to \infty$ yielding the uncharged ($q = 0$) Schwarzschild interior solution. We are not interested in negative a.

2. Exterior solution

The solution of Einstein-Maxwell field equations, Eqs. (6)-(8), for the external region, $r > r_0$, is given by

$$A(r) = \frac{1}{1 - \dfrac{2m}{r} + \dfrac{q^2}{r^2}}\,, \tag{24}$$

$$B(r) = \frac{1}{A(r)} = 1 - \frac{2m}{r} + \frac{q^2}{r^2}\,, \tag{25}$$

$$\phi(r) = \frac{q}{r}\,, \tag{26}$$

$$\rho_{\rm m}(r) = 0\,, \tag{27}$$

$$p(r) = 0\,, \tag{28}$$

$$\rho_{\rm e} = 0\,, \tag{29}$$

and the auxiliary functions are

$$M(r) = m\,, \tag{30}$$

$$Q(r) = q\,, \tag{31}$$

which is the Reissner-Nordström solution. Note that, by continuity on the surface $r = r_0$, the metric functions yield $B(r_0) = 1/A(r_0) = 1 - \dfrac{2m}{r_0} + \dfrac{q^2}{r_0^2}$. Also one must have $\phi(r_0) = \dfrac{q}{r_0}$, $M(r_0) = m$, and $Q(r_0) = q$, m and q being the total mass and total charge of the exterior spacetime.

3. Junction conditions

To do the matching properly, we start by imposing the junction condition that the metric should be continuous at the boundary surface $r = r_0$. In fact, by joining the interior metric function $g_{rr} = A(r)$ in Eq. (11) with the g_{rr} coefficient of the exterior metric given by (25), it is found [1] that

$$m = \frac{r_0}{2}\left(\frac{r_0^2}{R^2} + \frac{q^2}{r_0^2}\right). \tag{32}$$

Another junction condition arises by using the continuity of the $g_{tt} = B(r)$ metric coefficient, the continuity of its first derivative at $r = r_0$, and Eq. (8). Then one gets

$$a = \frac{r_0^2}{4q^2}\left(\frac{r_0^2}{R^2} - \frac{q^2}{r_0^2}\right)^2\left(1 - \frac{r_0^2}{R^2}\right)^{-1}. \tag{33}$$

where the fact that $Q(r_0) = q$ was also taken into account, and positive q is assumed without loss of generality.

4. Some constraints

Equations (32)-(33) are two constraints to the five free parameters of the solutions, a, R, m, q, and r_0. We now investigate some constraints on these parameters.

Using Eqs. (32)-(33) it is possible to treat the Guilfoyle parameter a and the mass m of the solution as a function of the other parameters of the theory, namely, $m = (r_0, R, q)$ and $a = a(r_0, R, q)$. Relation (33) implies a may be zero or negative in some range of the parameters. However, to avoid imaginary electromagnetic fields, we are interested just in solutions for which

$$a > 0\,, \tag{34}$$

and so we use Eq. (33) to constrain the range of the parameters r_0 and R. The condition $a > 0$ requires that

$$r_0 \leq R\,. \tag{35}$$

The constants k_0 and k_1 in Eqs. (20)-(21) are also found through the junction conditions.

C. Black hole conditions

We are looking for regular black holes. The conditions for the solutions to be regular are subtle and can be found numerically. The conditions for the solutions to be black holes are simple and can be stated now. The first condition to check is the presence of horizons. Namely, the expressions for the Cauchy and event horizon radii of the Reissner-Nordström solution exterior to the matter,

$$r_- = m - \sqrt{m^2 - q^2}\,, \tag{36}$$

$$r_+ = m + \sqrt{m^2 - q^2}\,, \tag{37}$$

respectively, have to produce real numbers. Then the overcharged solutions are discarded and we have the constraint,

$$m^2 \geq q^2\,. \tag{38}$$

Thus the existence of r_- and r_+ for the electrically charged solutions guarantees that the solutions are black holes.

Moreover, the radius of the boundary surface r_0 cannot be larger than, or at most, the gravitational radius r_+, i.e., $r_0 \leq r_+$. However, inequality (38) together with condition (35) imply that the value of r_0 cannot be in the region between r_- and r_+. Additionally, the boundary conditions impose that r_0 cannot be equal to r_+, with one special case as an exception, when $r_0 = r_-$ and at the extremal regime $m^2 = q^2$, which means $r_- = r_+ = r_0$. The constraint for r_0 is then

$$0 \leq r_0 \leq r_-\,, \tag{39}$$

the equality holding in the limit of $r_0 = R$. This result and Eq. (37) give

$$0 \leq r_0 \leq m\,, \tag{40}$$

the equality holding in the limit of $q = m$.

III. REGULAR NONEXTREMAL BLACK HOLES WITH CHARGED PHANTOM MATTER

In testing for regularity of the solutions, we find that there is a region of the parameter space which corresponds to regular black holes for small characteristic length R, namely,

$$0 < \frac{R}{q} \leq 1\,. \tag{41}$$

From now on we write the parameters of the problem as parameters without units, mainly we use the total charge q as the quantity to which the other parameters are gauged. Since from Eq. (10), $\rho_{\rm m}(r) + Q^2(r)/8\pi r^4 = 3/8\pi R^3 =$ constant, small characteristic length R means sufficiently large total energy density, i.e., the configurations are compact relative to the electric charge. Or, if one prefers, the configurations are heavily charged in comparison.

Besides R/q, another useful parameter for our analysis is the ratio r_0/R, which is the ratio of the radius of the matter distribution to the energy density parameter R. For very compacted charged spheres, typically, for $r_0/R \lesssim 0.9$, the fluid energy density $\rho_{\rm m}(r)$ assumes negative values at some r. On the other hand, for

$$\frac{r_0}{R} \simeq 1 \tag{42}$$

from below, the energy density $\rho_{\rm m}(r)$ is positive, while the pressure is negative everywhere inside the central core. For solutions in this range one has $p(r) < -\rho_{\rm m}(r)$, i.e.,

$$\rho_{\rm m}(r) + p(r) < 0\,, \tag{43}$$

which means that the fluid is composed of a phantom matter with electric charge. This is a Guilfoyle phantom fluid.

To show that these configurations are indeed black holes, regular ones, we focus on the physical quantities

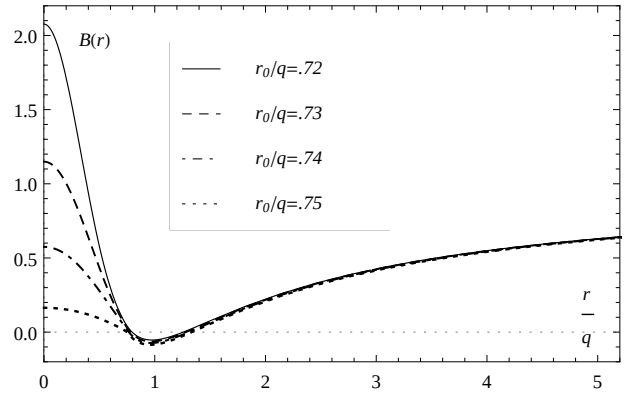

FIG. 1: Graphs of $B(r)$ for $R/q = 0.75$ and four different r_0/q: $r_0/q = 0.72$ (solid line), $r_0/q = 0.73$ (dashed line), $r_0/q = 0.74$ (dash-dotted line), and $r_0/q = 0.75$ (dotted line).

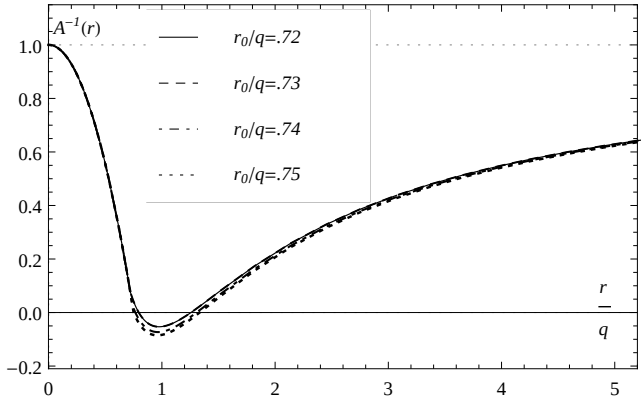

FIG. 2: Plots of $1/A(r)$ for $R/q = 0.75$ and four different r_0/q: $r_0/q = 0.72$ (solid line), $r_0/q = 0.73$ (dashed line), $r_0/q = 0.74$ (dash-dotted line), and $r_0/q = 0.75$ (dotted line).

$B(r)$, $A(r)$, $\rho_{\rm m}(r)$, $p(r)$, and $\rho_{\rm e}(r)$ and plot them as functions of r. The potential $\phi(r)$ is not necessary to plot as it is given by Eq. (13). We also plot $M(r)$ and $Q(r)$ which are useful quantities. As a typical class of configurations we consider the case

$$\frac{R}{q} = 0.75\,. \tag{44}$$

According to Eq. (35), the maximum value for r_0/q is $r_0/q = R/q$, so in this case the upper limit is then

$$\frac{r_0}{q} \leq 0.75\,. \tag{45}$$

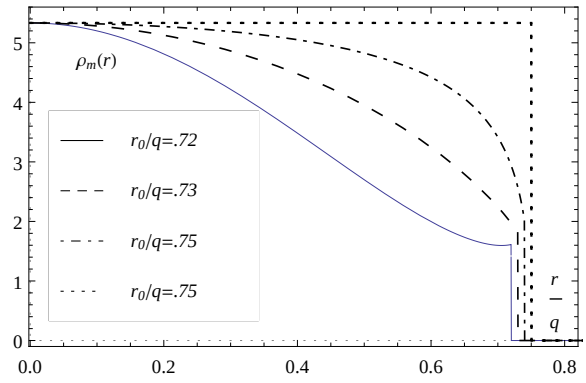

FIG. 3: A plot of the energy density $\rho_{\rm m}(r)$ for $R/q = 0.75$ and four different r_0/q: $r_0/q = 0.72$ (solid line), $r_0/q = 0.73$ (dashed line), $r_0/q = 0.74$ (dash-dotted line), and $r_0/q = 0.75$ (dotted line).

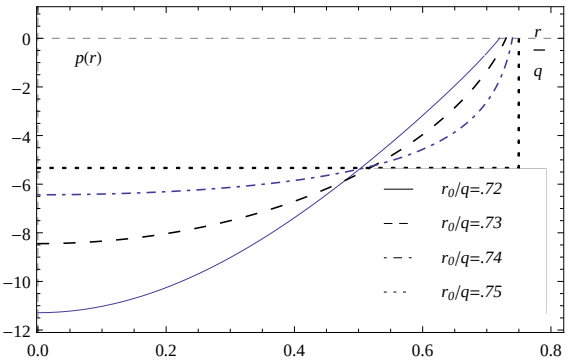

FIG. 4: A plot of the pressure $p(r)$ for $R/q = 0.75$ and four different r_0/q: $r_0/q = 0.72$ (solid line), $r_0/q = 0.73$ (dashed line), $r_0/q = 0.74$ (dash-dotted line), and $r_0/q = 0.75$ (dotted line).

In Figs. 1-7 we display the behavior as a function of r of the above-mentioned physical quantities for four different values of r_0/q, namely, $r_0/q = 0.72$, 0.73, 0.74, 0.75, this latter number being the maximum value possible, see Eq. (45).

In Figs. 1-2 the plots of the metric potentials $B(r)$ and $1/A(r)$ are shown. Clearly there are no curvature

singularities, i.e., the black holes are regular. The curve for $r_0/q = 0.75$ (dotted line) corresponds to a regular black hole with a de Sitter core, to be treated separately. The small difference among the curves of Figs. 1 and 2 is related to the fact that we considered regular black holes of almost the same sizes, i.e., with values of r_0/q very close to each other. Although the values of the mass m are relatively close to q, these regular black holes are far from being extremal as r_+ and r_- differ substantially. These facts can be found in Table I, which shows the values of the mass m, the Cauchy and event horizon radii, r_- and r_+, respectively, for some chosen values of r_0/q, with $R/q = 0.75$ fixed. It is clear from the table that $r_0 < r_-$, i.e., the matter radius is inside the Cauchy horizon.

r_0/q	$m(r_0, 0.75)/q$	$r_-(r_0, 0.75)/q$	$r_+(r_0, 0.75)/q$
0.720000	1.02622	0.795724	1.25672
0.730000	1.03072	0.780939	1.28051
0.740000	1.03587	0.765622	1.30613
0.750000	1.04167	0.750000	1.33333

TABLE I: Values of the mass m, Cauchy horizon r_- and event horizon r_+ in terms of the radius r_0 of the charged mass core of the regular black holes for $R/q = 0.75$, for four different values of r_0/q.

In Fig. 3 the energy density $\rho_{\rm m}(r)$ is displayed for the mentioned range of parameters. We see that within this range it is positive. The curve with $r_0/q = 0.75$ (dotted line) is flat, has a sharp drop at the boundary, and corresponds to a de Sitter core. Due to its particular interest it is studied separately. For smaller values of r_0 the solutions are less interesting, as they have negative energy densities. In Fig. 4 the pressure $p(r)$ is shown. The values are negative and higher in modulus than the energy density $\rho_{\rm m}(r)$. The fluid is a phantom fluid. The curve with $r_0/q = 0.75$ (dotted line), that is flat and drops sharply to zero at the boundary corresponds to a de Sitter core.

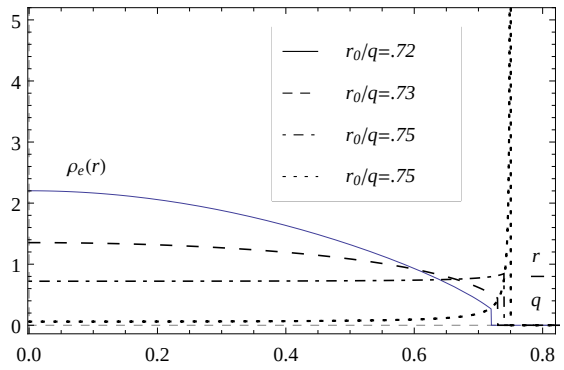

FIG. 5: A plot of the charge density $\rho_{\rm e}(r)$ for $R/q = 0.75$ and four different r_0/q: $r_0/q = 0.72$ (solid line), $r_0/q = 0.73$ (dashed line), $r_0/q = 0.74$ (dash-dotted line), and $r_0/q = 0.75$ (dotted line).

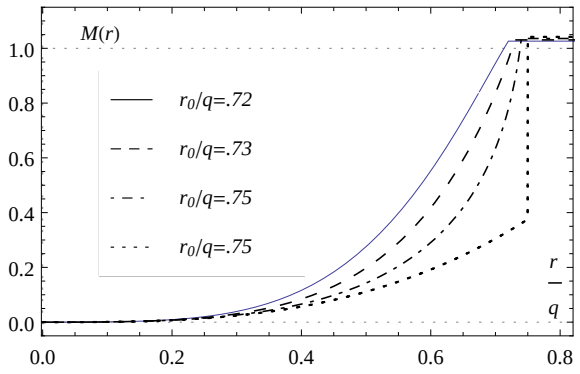

FIG. 6: A plot of the mass function $M(r)$ for $R/q = 0.75$ and four different r_0/q: $r_0/q = 0.72$ (solid line), $r_0/q = 0.73$ (dashed line), $r_0/q = 0.74$ (dash-dotted line), and $r_0/q = 0.75$ (dotted line).

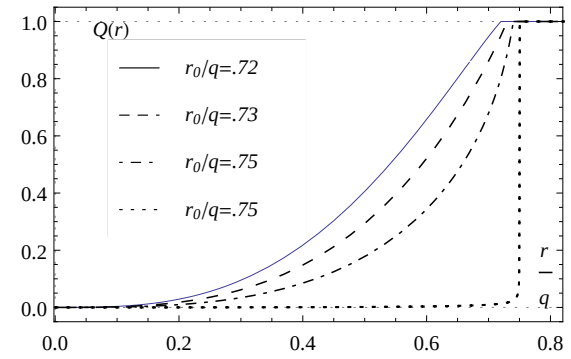

FIG. 7: A plot of the charge function $Q(r)$ for $R/q = 0.75$ and four different r_0/q: $r_0/q = 0.72$ (solid line), $r_0/q = 0.73$ (dashed line), $r_0/q = 0.74$ (dash-dotted line), and $r_0/q = 0.75$ (dotted line).

In Figs. 5 the charge density profiles $\rho_{\rm m}(r)$ for the given range of parameters are shown. Finally, the behavior of the auxiliary functions $M(r)$ and $Q(r)$ is shown in Figs. 6 and 7, respectively.

The conformal Carter-Penrose diagram of this regular black hole is shown in Fig. 8. The external region ($r > r_0$) is Reissner-Nordström, possessing a Cauchy and an event horizon, r_- and r_+, respectively. In the external region there are three distinct regions indicated in the figure by I, II, and III. The internal regular region, indicated by R in the diagram, is filled by a distribution of charged matter for which the pressure is negative and larger in absolute value than the energy density in the central core.

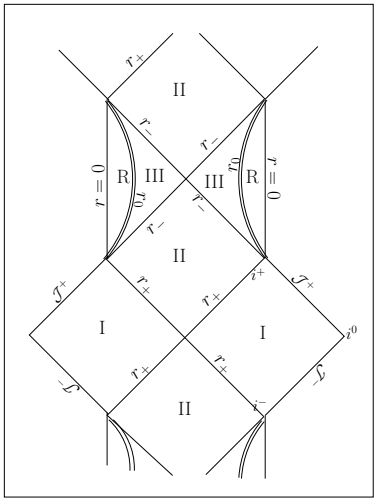

FIG. 8: The Carter-Penrose diagram for the regular nonextremal black hole with $r_0 < r_- < r_+$.

IV. REGULAR BLACK HOLES WITH A DE SITTER CORE AND A MASSLESS CHARGED LAYER AT THE CAUCHY HORIZON

Within this set of Guilfoyle solutions there are also regular black holes with a de Sitter core whose matching to the exterior region occurs at the Cauchy horizon, $r_0 = r_-$, which is a null, i.e., lightlike, surface. The interior fluid, $r < r_0 = r_-$, is uncharged, satisfying a de Sitter equation of state $p = -\rho_m = 3/8\pi R^2$, so that

$$\rho_{\rm m}(r) + p(r) = 0\,, \tag{46}$$

for this fluid. It is a false vacuum de Sitter core, the limiting case of a phantom fluid $\rho_m + p < 0$. The boundary of this de Sitter core, $r = r_0 = r_-$, is a layer of zero mass but nonzero charge. Thus, all the electric charge is on such a surface.

Let us show from the equations that this regular black hole solution exists.

By inspection, or otherwise, it is seen that this solution exists when $r_0 = r_-$. Since by Eq. (36), $r_- = m - \sqrt{m^2 - q^2}$, using Eq. (32), we obtain $r_0 = m(q, r_0, R) - \sqrt{m^2(q, r_0, R) - q^2} = q^2/2r_0 + r_0^3/2R^2 - \sqrt{\left(q^2/2r_0 + r_0^3/2R^2\right)^2 - q^2}$. This equation gives two solutions. One is $r_0 = r_- = 0$, which is satisfied for all $q^2 \geq 0$ and is in fact a singular black hole. The other solution is

$$r_0 = r_- = R\,, \tag{47}$$

and is satisfied only for $R/q < 1$. This latter is the solution that yields regular black holes. Thus

$$\frac{r_0}{q} = \frac{r_-}{q} = \frac{R}{q} < 1\,, \tag{48}$$

for this black hole.

Let us now discuss the features of the three different regions of this regular black hole.

(i) The region $r < r_0 = r_- = R$: In this region the interior fluid is uncharged, satisfying a de Sitter equation of state.

Indeed, in the limit $r_0 \to R$ the ratio $-p(r)/\rho_{\rm m}$ tends to unity, $p = -\rho_m = 3/8\pi R^2$. One can find this result by taking the limit $r_0 \to R$ in Eqs. (12)-(21) with the help of Eqs. (32)-(33).

To be specific, we see from Eq. (33) that for $r_0 = R$ and for $r_0/q < 1$, see Eq. (48), the parameter $a(r_0, R)$ diverges with $(1 - r_0^2/R^2)^{-1}$. Hence, Eq. (20) implies that the following limit, $\lim_{r_0 \to R} k_0(r_0, R) = \dfrac{R^2}{r_0^2}\left(\dfrac{m}{r_0} - \dfrac{q^2}{r_0^2}\right)$, is finite. Similarly, it follows from Eq. (21) that the constant k_1 goes to zero with $\sqrt{1 - r_0^2/R^2}$. Therefore, for $r \neq R$, the function $F(r)$ defined in Eq. (19) is finite and nonzero. Then, in the limit $r_0 \to R$ the solution for $r < r_0$ is

$$B(r) = \frac{1}{4}\left(1 - \frac{q^2}{r_0^2}\right)^2\left(1 - \frac{r^2}{R^2}\right)$$

$$= \frac{1}{4}\left(1 - \frac{q^2}{r_0^2}\right)^2 A^{-1}(r)\,, \quad r < r_0\,, \tag{49}$$

$$8\pi\,\rho_{\rm m}(r) = -8\pi\,p(r) = \frac{3}{R^2}\,, \quad r < r_0\,, \tag{50}$$

$$Q(r) = 0\,, \quad r < r_0\,. \tag{51}$$

Thus these black holes have a central de Sitter vacuum up to r_0, $r < r_0$.

Note that generically, the metric function $B(r)$ can be made equal to $1/A(r)$ by a redefinition of the time coordinate. Note also that for $r_0/q = 1$, a case that follows outside the configurations we are studying (see Eq. (48)), $B(r) = 0$ for all $r < r_0$ and we are in the presence of a quasiblack hole.

(ii) The region $r = r_0 = r_- = R$: In this region one has an electrically charged massless layer. Indeed, in the limit $r_0 \to R$, and $r_0/q < 1$ the function $F(r)$ defined in Eq. (19) goes to zero as $\sqrt{1 - r_0^2/R^2}$. Then the charge density diverges at $r = r_0 = R$, but the total charge is finite,

$$Q(r = r_0) = q\,, \quad r = r_0\,. \tag{52}$$

(iii) The region $r > r_0 = r_- = R$: By construction this region is the Reissner-Nordström vacuum.

Thus, we have shown that a regular black hole solution

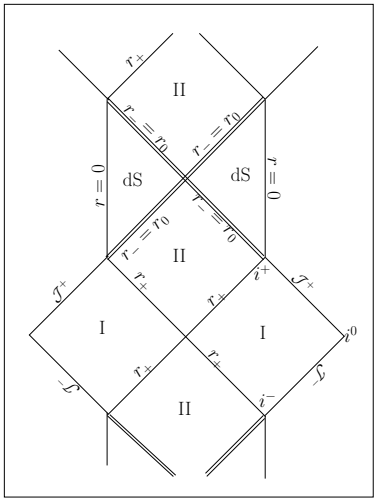

FIG. 9: The Carter-Penrose diagram for the regular black hole with a de Sitter central core and a lightlike matter boundary at the Cauchy horizon, where $r_0 < r_-$.

with a de Sitter core and a massless electrically charged layer at the Cauchy horizon is a solution of the equations.

The resulting metric and fluid functions for this extremal case correspond to the dotted curves of Figs. 1-7. Those plots show the particular case $r_0/q = R/q = 0.75$. Worth noting is the graph for $\rho_e(r)$ (dotted curve of Fig. 5), which is essentially 0 for $0 \leq r < r_0$, and diverges at $r = r_0$. Its integration gives $Q(r)$, see Fig. 7, i.e., it is zero for $r < r_0$ and q for $r \geq r_0$, indicating that ρ_e has similar properties to the Dirac delta function. This special case is identical to a special case of the regular charged black holes found in [8], see also [10]. The conformal Carter-Penrose diagram for these regular black holes is shown in Fig. 9. In the external region there are two distinct regions indicated in the figure by I and II. The internal regular region, indicated by dS in the diagram, the de Sitter core, is fulfilled by an uncharged fluid with equation of state of de Sitter type, $p = -\rho_m$.

V. THE SPACE OF PARAMETERS: LOOKING FOR ALL REGULAR BLACK HOLES

A. Generics

The model has five free parameters, m, q, r_0, R, and a, and two relations among them (Eqs. (32) and (33)). In summary, we have five parameters and only two constraints so that three parameters are left free. Here we choose r_0, R, and q as free parameters. We normalize all quantities in terms of q, which is equivalent to setting the charge q to unity.

In the two previous sections we studied two typical classes of regular black holes within the Guilfoyle solutions. Now, we investigate the space of parameters where regular black holes can be found. For this, we start by showing the dependence of the Guilfoyle parameter a and of the mass m as a function of the other parameters of the model. After that we show all the different regions containing regular black holes.

B. The mass m and the Guilfoyle parameter a

1. *The mass function m*

From Eq. (32) it follows that the ratio m/q is a function of the two parameters r_0/q and R/q. Figure 10 shows the mass m/q of each configuration as a function of r_0/q for five different values of R/q. Since r_0 cannot be larger than R, all the plotted curves in such a figure end at $r_0 = R$.

Based on Eq. (32) and Fig. 10 we find that there is an important value for R/q, namely, $R/q = 4\sqrt{3}/9$, with $4\sqrt{3}/9 \simeq 0.77$. We can then divide the analysis of the mass properties m/q into three cases depending on the values of R/q: (i) $0 < R/q < 4\sqrt{3}/9$, (ii) $R/q = 4\sqrt{3}/9$, and (iii) $4\sqrt{3}/9 < R/q < \infty$.

(i) $0 < R/q < 4\sqrt{3}/9$: In this region there appears also another important value for R/q, $R/q = \sqrt{3}/3$, with $\sqrt{3}/3 \simeq 0.56$. (a) For $0 < R/q < \sqrt{3}/3$ all of the curves end abruptly when $a = 0$ (the region of the parameter space where the Guilfoyle parameter a assumes negative values is not considered in the present work as for these values the electric charge is imaginary). This happens, e.g., in the case of the curve for $R/q = 0.3$, see Fig. 10, which ends at an r_0 given by $r_0/q = 0.3$. (b) For $R/q = \sqrt{3}/3$ one finds the curve for which the minimum coincides exactly with the endpoint of the line. This curve is not shown in Fig. 10, because it would cause a mess in the figure. (c) For $\sqrt{3}/3 < R/q < 4\sqrt{3}/9$ and for fixed R/q the mass function $m(r_0, R)$ has a minimum at some finite value of r_0, see Fig. 10. This minimum is denoted by $\bar{r}_0$. Now, Eq. (32) furnishes for this minimum the value $\bar{r}_0/q = \sqrt[4]{R^2/3q^2}$. The corresponding minimum value of the mass, $\bar{m} = m(\bar{r}_0, R)$, is such that $\bar{m}\bar{r}_0 = 2q^2/3$. Thus, in brief, within this range, for fixed R/q, we see that as r_0/q increases the mass m/q increases if $r_0/q > \sqrt[4]{R^2/3q^2}$ and the mass m/q decreases if $r_0/q < \sqrt[4]{R^2/3q^2}$. The increasing of the mass m with r_0 for large r_0 is expected, because with R/q fixed, i.e., with the energy density fixed, the mass-energy increases with the size of the object. On the other hand, the decreasing of m with r_0 for small r_0 may be understood by noticing that in this case the total mass is dominated by

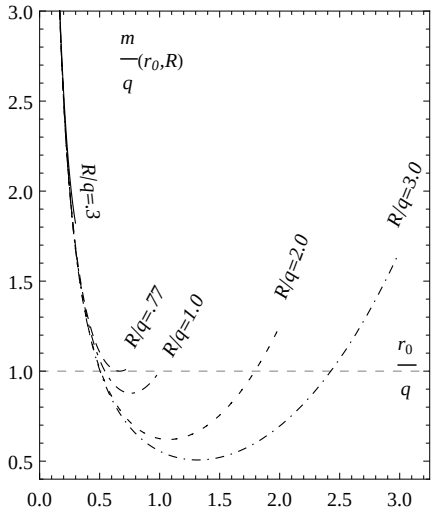

FIG. 10: A plot of the mass m/q as a function of r_0/q for different values of R/q, as shown in the curves.

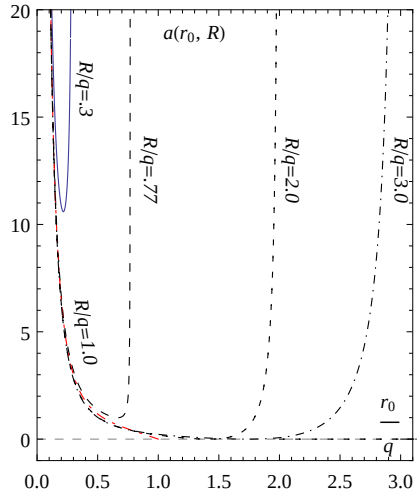

FIG. 11: A plot of the parameter a as a function of r_0/q for different values of R/q. All the curves have two branches, one for positive values and the other for negative values. The branches of negative values are not shown. The function $a(r_0/q, R/q)$ is singular at $r_0/q = R/q$. The only exception is for $R/q = 1$, which gives $a(r_0/q, R/q) = 0$.

the electromagnetic energy, $q^2/2r_0$, which decreases with increasing r_0.

(ii) $R/q = 4\sqrt{3}/9$: For this value the minimum of the curve m/q coincides with the value $m/q = 1$. This minimum limit is found at $\bar{r}_0/q = 2/3$, see Fig. 10.

(iii) $4\sqrt{3}/9 < R/q < \infty$: In this case the value of $\bar{r}_0$ is larger than $\bar{r}_0/q \simeq 0.42$ and the respective masses are such that $m/q \leq 1$. In fact there is a range of values of r_0 for which $m/q \leq 1$, meaning these objects are overcharged or are extremal. Overcharged objects certainly do not represent regular black holes and are not of interest for the present work. Extremal black holes that are regular could not be found in these solutions. Thus, only configurations that satisfy $m/q > 1$ can be regular black holes. Within this range of R/q we see that regular black holes can exist in the two disjoint parts of the curve for which $m/q \geq 1$. An example is $R/q = 2$. It has $\bar{r}_0/q = \sqrt[4]{4/3}$, and $\bar{m}/q = \sqrt[4]{12}/3 < 1$, see Fig. 10.

2. *The Guilfoyle parameter a*

Typical curves for the parameter a as a function of r_0/q and R/q are shown in Fig. 11. For fixed R/q one has that all the curves show a smooth branch in the form of a cup. The curves have a minimum at some value of r_0, $\tilde{r}_0$ say (the root of a polynomial), and tend to $+\infty$ at $r_0 \to 0$ and $r_0 \to R$. Examples of these are the curves for $R/q = 0.3$, $R/q = 0.77$, $R/q = 2.0$, and $R/q = 3.0$ in Fig. 11. The case $R/q = 1$ is special in the sense that the curve has no local minimum and ends at $r_0/q = 1$.

C. Regions of the parameter space and general properties of the solutions

In the following we list the different regions of the parameter space $(r_0/q, R/q)$ in which the corresponding solutions represent regular black holes.

1. $0 \leq R/q < 4\sqrt{3}/9$: *High mass-energy densities*

For sufficiently compact charged mass distributions, i.e., high mass-energy densities, R/q is in the range $0 \leq R/q < 4\sqrt{3}/9 \simeq 0.77$. A typical case in this range is shown in Fig. 12 for $R/q = 0.75$. Particular instances of r_0/q within this case were studied in Sec. III.

In Fig. 12 we plot the horizon radius r_+ and the Cauchy horizon r_- in terms of r_0/q for $R/q = 0.75$. There are regular black holes for all values of r_0/q.

The dependence of the mass m and of the parameter a in terms of r_0/q for this $R/q = 0.75$ case is similar to the curves indicated by $R/q = 0.3$ and $R/q = 0.5$ in Figs. 10 and 11, respectively. One notes that the mass is larger than the charge for all these objects. Also for these large mass-energy density objects there are always two horizons, the event horizon r_+ and the Cauchy inner horizon r_- which cannot be equal to each other, $r_+(r_0, R) > r_-(r_0, R)$. Thus there are no extremal black holes. The boundary of the matter core r_0 can be equal to the Cauchy horizon only when $r_0 = R$ ($r_0 = 0$ is

excluded because it gives singular solutions). Solutions belonging to this region of the parameter space may be regular black holes with a timelike boundary below the inner horizon, or, if $r_0 = R$, with a lightlike boundary at the inner horizon, see Secs. III-IV.

The good regular black holes, i.e., the ones with non-negative fluid energy density, are found for r_0/q close to R/q. Such a kind of situation is shown by the particular solutions whose metric, energy density pressure, and charge density functions are plotted in Figs. 1-7.

The solutions for small r_0 tend to behave badly in the sense that the pressure $p(r)$ assumes very large negative values in some regions. In the same situations, the energy density of the fluid $\rho_{\rm m}(r)$ may also become negative in some regions.

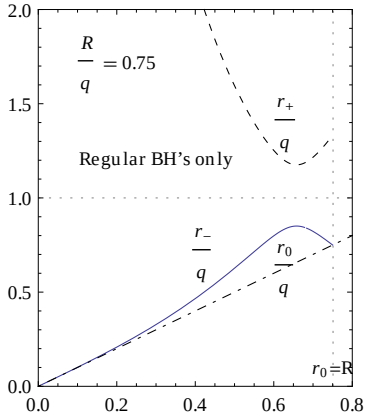

FIG. 12: A plot of r_+/q and r_-/q as a function of r_0/q for $R/q = 0.75$, the case explored in Sec. V

.

2. $R/q = 4\sqrt{3}/9$: *Special case for the mass-energy density*

The dependence of the mass m in terms of r_0/q for this $R/q = 4\sqrt{3}/9 \simeq 0.77$ case is indicated in Fig. 10, see also Fig. 11 for the dependence of a. The mass is larger than the charge for all these objects, except at the extremal value, $r_0/q = 2/3$, for which the mass equals the electric charge and the two horizon radii are identical, $r_+/q = r_-/q = 1.0$.

The plots of the radii $r_\pm/q$ in terms of r_0/q for this special value of R/q are shown in Fig. 13. For $r_0/q \neq 2/3$, the class of solutions corresponding to this region presents similar properties to the case of Fig. 12. The solutions for $R/q = 4\sqrt{3}/9 \simeq 0.77$ are regular black holes for all r_0/q ($0 < r_0/q \leq R/q$).

The boundary surface r_0 of the matter is timelike for all $r_0/q < R/q$, and is lightlike for $r_0/q = R/q$. The nonextremal regular black holes with $r_0/q < R/q$ (and $r_0/q \neq 2/3$) all have the same causal structure as shown in the conformal diagram of Fig. 8, and, for values of r_0/q sufficiently close to R/q, the matter content of these regular black holes satisfy a phantom-type equation of state.

The regular black holes with a lightlike boundary at $r_0/q = R/q$ are those with a de Sitter core and a charged layer at r_0. These were studied in detail in Sec. IV.

For $r_0/q = 2/3$ the event and the Cauchy horizons coincide and we find a regular extremal black hole although it has negative energy density in some regions in the central core and we do not dwell further on it.

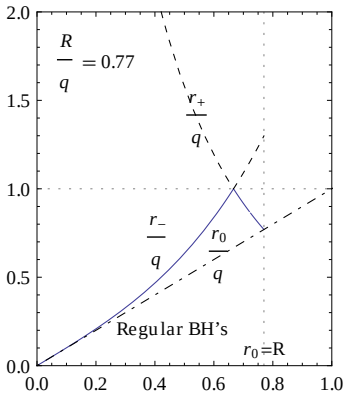

FIG. 13: A plot of r_+/q and r_-/q as a function of r_0/q for $R/q = 4\sqrt{3}/9 \simeq 0.77$. The horizons coincide at $r_0/q = 2/3$ for which $r_+/q = r_-/q = 1$.

3. $4\sqrt{3}/9 < R/q < \infty$: *Intermediate and low mass-energy densities*

(i) $4\sqrt{3}/9 < R/q < 1$: Intermediate energy densities

For more disperse, not so compact, charged mass distributions, R/q is in the range $4\sqrt{3}/9 < R/q < 1$. A typical case in this range is shown in Fig. 14 for $R/q = 0.78$.

In Fig. 14 we plot the horizon radius r_+ and the Cauchy horizon r_- in terms of r_0/q for $R/q = 0.78$. There are regular black holes for some values of r_0/q.

The behavior of the mass function $m(r_0/q, R/q)$ is similar to the curve for $R/q = 1$ in Fig. 10. Given a value of R/q within this interval, the minimum of the corresponding curve is at $\bar{r}_0/q = \sqrt[4]{R^2/3q^2}$, which is in the interval $2/3 \leq \bar{r}_0/q \leq \sqrt[4]{3}$ and the values of the mass are bounded from below by $\bar{m}/q \simeq 0.877$.

The regular black holes in the region $0 < r_0/q < 0.63$ suffer from the drawback of presenting negative energy density in some region inside matter, i.e., $\rho_{\rm m}(r)$ assumes negative values for some r. For r_0/q in the interval $0.63 <$

$r_0/q < 0.71$ the solutions correspond to overcharged stars (regular and in some cases singular). Finally, in the last region, $0.71 < r_0/q < 1$, well-behaved regular black holes are found with positive $\rho_{\rm m}(r)$ and phantom matter.

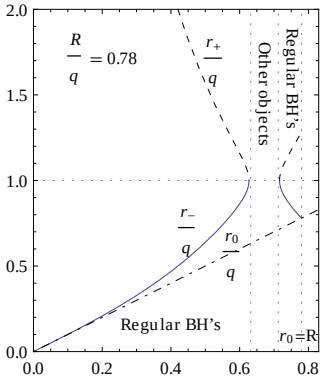

FIG. 14: A plot of r_+/q and r_-/q as a function of r_0/q for $R/q = 0.78$. The first vertical dashed line is at $r_0/q \simeq 0.63$, and the second one is at $r_0/q \simeq 0.71$.

(ii) $R/q = 1$: A special case with intermediate mass-energy density

An interesting special intermediate mass-energy density case is the one that has $R/q = 1.0$.

In Fig. 15 we plot the horizon radius r_+ and the Cauchy horizon r_- in terms of r_0/q for $R/q = 1.0$. The regular black holes are found in these Guilfoyle solutions in the region $0 < r_0/q \lesssim 0.55$, the largest matching $r_0 \sim 0.55$ occurs in the extremal black hole case, $r_- = r_+$. For solutions in this range the mass-energy density is negative in some regions inside matter for solutions with small r_0 when compared to R. Hence, these are not good regular black holes.

Also, for $R/q = 1$ in the limit $r_0/q \to R/q$ a quasiblack hole is found. This is shown in Fig. 15 by the point indicated by QBH. We comment further on this solution. As mentioned above, the maximum possible value of r_0 is the de Sitter radius R, $r_0 = R$. In that limit, Eq. (32) implies $1-2m/r_0+q^2/r_0^2 = 0$, meaning that the boundary surface coincides with a horizon of the exterior metric. More precisely, the matching is done at the inner horizon of the exterior Reissner-Nordström spacetime, $r_0 = r_-$, with the event horizon r_+ being outside the matching surface. The only exception is the extremal case $m^2 = q^2$, for which one has also $r_- = r_+$, and then $r_0 = r_+$. This case is represented by the point QBH in Fig. 15, where the matching is at $r_0/R = q^2/R^2 = 1$, and with $r_- = r_+$. In fact, this is not a regular black hole. This is the quasiblack hole case [3]. The same type of solution was reported in [8].

(iii) $1 < R/q < \infty$: Low mass-energy densities

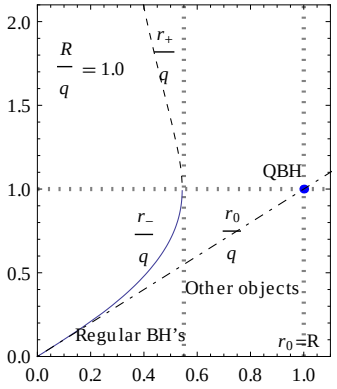

FIG. 15: A plot of r_+/q and r_-/q as a function of r_0/q for $R/q = 1.0$. The point indicated by QBH is the quasiblack hole solution.

For disperse, low mass-energy density distributions, R/q is in the range $1 < R/q < \infty$. A typical case in this range is shown in Fig. 16 for $R/q = 3.0$.

In Fig. 16 we plot the horizon radius r_+ and the Cauchy horizon r_- in terms of r_0/q for $R/q = 3.0$. As in the case of Fig. 14, there are two branches for r_+ and r_-. One branch ends at $r_0/q \simeq 0.51$ and the other starts at $r_0/q \simeq 2.42$. There are regular black holes for sufficiently small r_0/q. The vertical dotted line at $r_0/q \simeq 0.51$ is drawn to indicate that the regular black hole region ($r_0/q \leq r_-/q$) is on the left of that point, i.e., there are regular black holes just for $0 < r_0/q \lesssim 0.51$. In the whole region $0.51 \lesssim r_0/q \leq R/q$ there are other kinds of objects, overcharged objects for $0.51 \lesssim r_0/q < 2.42$, undercharged stars for $2.42 \lesssim r_0/q \lesssim 2.8$, and singular objects above this value, i.e., for $2.8 \lesssim r_0/q < 3.0$ only singular objects are found.

Note that the matching is at $r = r_0$ and then the curves for $r_-(r_0, R)$ and $r_+(r_0, R)$ to the right of the vertical line at $r_0/q \simeq 2.42$ in Fig. 16 are not real horizons, because they would be inside the matter.

When $r_0 = R$ the boundary is at $r_0 = R = r_+$, i.e., at the horizon. However, for r_0 close to R the solutions are singular at one or several radii r. Thus, we do not analyze objects with r_0 close to R.

Again, the region where regular black holes may be found corresponds to relatively small values of the matter boundary radius r_0. This means that the pressure assumes very large negative values in some regions, and, moreover, the energy density also becomes negative in some regions inside matter. This drawback makes these regular solutions less interesting than the ones occurring for large energy density (with $R/q < 1$).

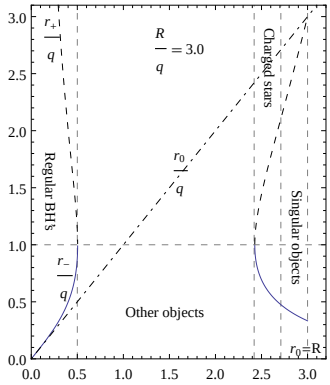

FIG. 16: A plot of r_+/q and r_-/q as a function of r_0/q for $R/q = 3.0$, a typical small energy density value.

D. Comments

Two other interesting features should be mentioned.

(i) The limit of zero r_0, for fixed R/q, gives singular charged black holes.

(ii) The limit of zero charge, with nonzero r_0, of these solutions is not regular black holes, but corresponds to uncharged stars for a given range of parameters. The exception is the limit of zero charge and zero r_0 that gives a Schwarzschild black hole.

E. On the numerical techniques employed

The starting point for the analysis is a system of relations defining the metric potentials $A(r)$ and $B(r)$ that define the spacetime geometry, and the other quantities that comprise the energy-momentum tensor; namely, the fluid quantities $\rho_m(r)$, $p(r)$, and U^μ, and the electromagnetic energy density $Q^2(r)/r^4$. These quantities are given in terms of three free parameters r_0, q, and R representing the radius, the electric charge, and a characteristic length related to the total energy density of the fluid. After normalizing with respect to q, we are left with two free parameters from what the other important parameters such as the mass m, horizons radii r_+ and r_-, and Guilfoyle parameter a are obtained, i.e., each nonfree parameter is treated as a function of the two free parameters, $m = m(r_0/q, R/q)$, etc., while the potentials and fluid quantities depend also on the radial coordinate r, $A(r) = A(r_0/q, R/q, r/q)$, and so on.

Since we have analytical expressions for all these quantities, the related numerical techniques employed to investigate the behavior of each functions are mainly visualization of graphics and approximation techniques, numerical or analytical.

The region where black holes are found is given by the conditions $m^2 > q^2$ and $r_0 \leq r_-$. Equations (32) and (37) help to locate such a region. Then, after choosing a specific pair of parameters $(r_0/q, R/q)$ satisfying these constraints, all the relevant functions are analyzed for the required physical conditions, in particular, the regularity of the energy density, pressure and electromagnetic energy density for all values of the radial coordinate r. The curvature scalars are also checked. This is done by using standard methods of functional analysis. We repeated the process by varying the two free parameters r_0/q and R/q along the appropriate region of the parameter space.

In summary, all the numerical and graphical analysis may be done using built in functions of the chosen algebraic software, e.g., using the internal functions of Wolfram Mathematica.

VI. CONCLUSIONS

Charged regular black holes have been found here for a range of parameters of the static spherically symmetric solutions displayed by Guilfoyle. For a range of parameters, the solutions are regular electrically charged black hole solutions. They are built from charged phantom matter satisfying the condition $\rho_{\rm m} + p \leq 0$ up to r_0. The metric for $r < r_0$ is regular and the isotropic pressure goes to 0 at r_0 while the energy density and the charge density may present discontinuities at r_0. The exterior is the Reissner-Nordström solution. The matter boundary is timelike and is always at a radius smaller than the inner Reissner-Nordström Cauchy horizon.

In the limiting case where $\rho_{\rm m}+p = 0$ the interior can be interpreted as a false vacuum de Sitter state. In this case, the isotropic pressure and the energy density are constant throughout the interior region. The boundary is lightlike, located at the inner Reissner-Nordström Cauchy horizon r_-. All the electric charge of the solution is located at this boundary.

Acknowledgments

JPSL thanks Fundação para a Ciência e Tecnologia (FCT), Portugal, for financial support through Grant No. UID/FIS/00099/2013. VTZ thanks Fundação Calouste Gulbenkian for financial support. VTZ also thanks Fundação de Amparo à Pesquisa do Estado de São Paulo (FAPESP) and Conselho Nacional de Desenvolvimento Científico e Tecnológico of Brazil (CNPq) for financial help. We thank Coordenação de Aperfeiçoamento do Pessoal de Nível Superior (CAPES), Brazil, Grant No. 88881.064999/2014-01.

[1] B. S. Guilfoyle, "Interior Weyl-type solutions to the Einstein-Maxwell field equations", Gen. Relativ. Gravit. **31**, 1645 (1999); arXiv:gr-qc/9906089.

[2] J. P. S. Lemos and V. T. Zanchin, "Electrically charged fluids with pressure in Newtonian gravitation and general relativity in d spacetime dimensions: Theorems and results for Weyl type systems", Phys. Rev. D 80, 024010 (2009); arXiv:0905.3553 [gr-qc].

[3] J. P. S. Lemos and V. T. Zanchin, "Quasiblack holes with pressure: Relativistic charged spheres as the frozen stars", Phys. Rev. D **81**, 124016 (2010); arXiv:1004.3574 [gr-qc].

[4] J. P. S. Lemos and V. T. Zanchin, "Sharp bounds on the radius of relativistic charged spheres: Guilfoyle's stars saturate the Buchdahl-Andréasson bound", Classical Quantum Gravity **32**, 135009 (2015); arXiv:1505.03863 [gr-qc].

[5] 28] J. M. Bardeen, "Non-singular general-relativistic gravitational collapse", in Abstracts of the 5th international conference on gravitation and the theory of relativity, edited by V. A. Fock et al. (Tbilisi University Press, Tbilisi, 1968), p. 174.

[6] E. Ayón-Beato and A. García, "The Bardeen model as a nonlinear magnetic monopole", Phys. Lett. B **493**, 149 (2000); arXiv:gr-qc/0009077.

[7] I. G. Dymnikova, "Vacuum nonsingular black hole", Gen. Relativ. Gravit. **24**, 235 (1992).

[8] J. P. S. Lemos and V. T. Zanchin, "Regular black holes: Electrically charged solutions, Reissner-Nordström outside a de Sitter core", Phys. Rev. D 83, 124005 (2011); arXiv:1104.4790 [gr-qc].

[9] N. Uchikata, S. Yoshida, and T. Futamase, "New solutions of charged regular black holes and their stability", Phys. Rev. D **86**, 084025 (2012); arXiv:1209.3567 [gr-qc].

[10] C. Barrabès and W. Israel, "Thin shells in general relativity and cosmology: The lightlike limit", Phys. Rev. D **43**, 1129 (1991).

[11] J. Matyjasek, D. Tryniecki, and M. Klimek, "Regular black holes in an asymptotically de Sitter universe", Mod. Phys. Lett. A **23**, 3377 (2008); arXiv:0809.2275 [gr-qc].

[12] L. Balart and E. C. Vagenas, "Regular black holes with a nonlinear electrodynamics source", Phys. Rev. D **90**, 124045 (2014); arXiv:1408.0306 [gr-qc].

[13] M.-S. Ma, "Magnetically charged regular black hole in a model of nonlinear electrodynamics", Ann. Phys. (N.Y.) **362**, 529 (2015); arXiv:1509.05580.

[14] A. Flachi and J. P. S. Lemos, "Quasinormal modes of regular black holes", Phys. Rev. D **87**, 024034 (2013); arXiv:1211.6212 [gr-qc].

[15] B. Toshmatov, A. Abdujabbarov, Z. Stuchlík, and B. Ahmedov, "Quasinormal modes of test fields around regular black holes", Phys. Rev. D **91**, 083008 (2015); arXiv:1503.05737 [gr-qc].

[16] J. Aftergood and A. DeBenedictis, "Matter conditions for regular black holes in $f(T)$ gravity", Phys. Rev. D **90**, 124006 (2014); arXiv:1409.4084 [gr-qc].

[17] M. E. Rodrigues, E. L. B. Junior, G. T. Marques, and V. T. Zanchin, "Regular black holes in $f(R)$ gravity", arXiv:1511.00569 [gr-qc].

[18] A. B. Balakin, J. P. S. Lemos, and A. E. Zayats, "Regular nonminimal magnetic black holes in spacetimes with a cosmological constant", Phys. Rev. D **93**, 024008 (2016); arXiv:1512.02653 [gr-qc].

[19] K. A. Bronnikov and J. C. Fabris, "Regular phantom black holes", Phys. Rev. Lett. **96**, 251101 (2006); arXiv:gr-qc/0511109.

[20] K. A. Bronnikov, H. Dehnen, and V. N. Melnikov, "Regular black holes and black universes", Gen. Relativ. Gravit. **39**, 973 (2007); arXiv:gr-qc/0611022.

[21] G. Clément, J. C. Fabris, and M. E. Rodrigues, "Phantom black holes in Einstein-Maxwell-dilaton theory", Phys. Rev. D **79**, 064021 (2009); arXiv:0901.4543 [hep-th].

[22] M. Azreg-Aïnou, G. Clément, J. C. Fabris, and M. E. Rodrigues, "Phantom black holes and sigma models", Phys. Rev. D **83**, 124001 (2011); arXiv:1102.4093 [hep-th].

[23] K. A. Bronnikov, R. A. Konoplya, and A. Zhidenko, "Instabilities of wormholes and regular black holes supported by a phantom scalar field", Phys. Rev. D **86**, 024028 (2012); arXiv:1205.2224 [gr-qc].

[24] S. V. Bolokhov, K. A. Bronnikov, and M. V. Skvortsova, "Magnetic black universes and wormholes with a phantom scalar", Classical Quantum Gravity **29**, 245006 (2012); arXiv:1208.4619 [gr-qc].

[25] K. A. Bronnikov and S. G. Rubin, *Black holes, Cosmology and Extra Dimensions* (World Scientific, Singapore, 2013).

[26] E. F. Eiroa and C. M. Sendra, "Regular phantom black hole gravitational lensing", Phys. Rev. D **88**, 103007 (2013); arXiv:1308.5959 [gr-qc].

[27] M. Akbar and O. Kittaneh, "Accretion of phantom energy by the Bardeen black hole", Int. J. Theor. Phys. **53**, 1953 (2014).

[28] M. Azreg-Aïnou, G. T. Marques, and M. E. Rodrigues, "Phantom black holes and critical phenomena", J. Cosmol. Astropart. Phys. (JCAP) **07**, 036 (2014); arXiv:1405.5745 [gr-qc].